Sea Ice Observed at Enhanced Resolution by Spaceborne Scatterometers

D. G. Long *D. Early*

Electrical and Computer Engineering Dept., 459 Clyde Build., Brigham Young University, Provo, UT 84602

Abstract - **Spaceborne scatterometers such as the Seasat-A (SASS) and the ERS-1 Active Microwave Instrument (AMI) scatterometers measure the radar backscatter of the earth's surface at a resolution of approximately 50 km. While adequate for studying winds over the ocean, the low resolution limits the utility of the scatterometer data for land and ice studies. However, by using a recently developed resolution enhancement algorithm we have been able to produce a time series of enhanced resolution radar backscatter of sea ice in the southern polar region. The images dramatically reveal seasonal change in the sea ice. Large-scale circulation and mixing patterns are evident and the ice edge is readily discernible. Comparisons between Ku-band (SASS) images and C-band (ERS-1) images are made. Our results suggest that scatterometer data coupled with the resolution enhancement technique is useful in sea ice studies. The frequent, multiple-incidence angle revisits may provide the capability to map ice age and snow cover.**

I. INTRODUCTION

Radar remote sensing is a proven technique for the study of polar ice from space. Traditionally, synthetic aperture radars (SARs) have been a primary tool for radar studies of the polar regions. However, while the high resolution of SARs is well-suited for focused-area studies, their narrow swath and limited temporal coverage have precluded their use in frequent, large-scale monitoring. Wider, more frequent coverage is required to achieve the desired goals in monitoring polar ice. Such comprehensive coverage can be obtained by using wind scatterometers. Scatterometers are low resolution (~50 km) real aperture radars originally designed to measure the backscatter of the ocean's surface in order to calculate the near-surface wind. They have very wide swaths (500-1000 km) and make measurements of the backscatter at a diversity of azimuth and incidence angles. While the low resolution of the scatterometer data has limited the application of the data, a recently developed resolution enhancement algorithm can be applied to produce images of the surface backscatter at resolutions as fine as 4 km [4]. This algorithm has been used successfully with SASS data to study the Greenland ice sheet by Long and Drinkwater [1993]. Using simple scattering models, they were able to identify and map key ice facies over virtually all of Greenland over the summer through fall seasons in 1978.

This work was supported by the National Aeronautics and Space Administration (NASA) programs in Physical Oceanography (David Adamec) and Polar Sciences (Robert Thomas).

In this paper we apply the resolution enhancement algorithm to both SASS and ERS-1 scatterometer data to create enhanced resolution (3-5 km) backscatter images of Antarctic sea ice. This paper is organized as follows: first, we briefly consider backscattering from sea ice and discuss the resolution enhancement technique. We then present sample images from an image time series covering July through early October 1978 for SASS data and July through October 1992 for ERS-1 data. We conclude with some observations and conclusions regarding the images and their utility.

II. RADAR BACKSCATTER FROM SEA ICE

SASS made 14.6 GHz measurements of hh- and vv-polarized σ^o on ascending and descending orbits at various azimuth and incidence angles. The nominal resolution was approximately 50 km over an irregular grid with hexagonal resolution cells [4]. Measurements were made over two 500-700 km wide swaths. In the polar regions a given area was generally observed twice each day. SASS operated for 3 months in 1978. The ERS-scatterometer, which is currently operating, makes nominally 50-60 km resolution measurements of 5.6 GHz vv-polarized σ^o on a regular 25 km grid at three azimuth angles over a 500 km wide swath. Because the scatterometer transmitter is shared with the AMI SAR, there are frequent scatterometer data outages in the polar regions.

Both the Seasat and ERS-1 scatterometers observe σ^o over a wide range of incidence angles. σ^o is, however, a function of the measurement incidence angle θ. In the range $\theta \in [20°, 55°]$, σ^o (in dB) is approximately a linear function of θ, i.e.,

$$\sigma^o(\theta) = \mathcal{A} + \mathcal{B}(\theta - 40°) \qquad (1)$$

where the coefficients $\mathcal{A}$ and $\mathcal{B}$ depend on the ice scattering characteristics and polarization. $\mathcal{A}$ can be thought of as the 40° "incidence angle-normalized σ^o," while $\mathcal{B}$ describes the dependence of σ^o on θ. Due to the wide range in θ, we will use $\mathcal{A}$ and $\mathcal{B}$ rather than σ^o in our images. In Eq. (1), 40° represents the mean θ of the observations. σ^o may also be a function of the azimuth angle of the observation; however, this is not considered in this paper.

The radar scattering in sea ice is highly dependent on the characteristics of the ice [1,2,5,6]. Some of the physical characteristics of the ice which affect the backscatter include: ice age, snow cover, air bubbles, brine inclusions, and the presense of liquid water. For example, in one study during winter conditions [5] at a limited number of sample sites, it was determined that the σ^o at a 40° incidence angle (i.e., $\mathcal{A}$) is highly dependent on the ice

0-7803-1385-2/93/$3.00

age. For multi-year sea ice it was determined that $\mathcal{A}$ is approximately -8 ± 2 dB at Ku-band and approximately -19 ± 3 dB at C-band. First-year ice was much "darker" with σ^o approximately -24 ± 4 dB at Ku-band and approximately -27 ± 4 dB at C-band. While the responses of first-year and multi-year ice can appear quite different, these differences can be reduced in the presense of liquid water in a surface or subsurface snow layer. Liquid water changes the dielectric properties of snow and ice and regulates the reflection or transmission of the radar signals at the layer interfaces. This, in turn, may limit the contribution of scattering within lower layers. However, because the predominate scattering mechanisms are different for first-year and multi-year ice, it may be possible to distinguish the scattering mechanism by making multiple incidence angle measurements of the same region. Since the scatterometer makes σ^o measurements over a wide range of incidence angles, the scatterometer data may enable determination of the primary scattering mechanism and, hence, enable mapping of ice age.

In examining the images presented below, note that because penetration into the ice is frequency dependent, with lower frequencies exhibiting higher penetration, C-band "sees" a slightly different portion of the ice than does Ku-band.

III. IMAGING TECHNIQUE

The imaging technique used in this paper is the scatterometer image reconstruction algorithm with filtering (SIRF) developed in [4]. A complete description of these algorithms may be found in this reference. The technique uses multiple, overlapping measurements of σ^o and post-processing to improve the effective resolution. Images of $\mathcal{A}$ with resolution up to 3-5 km from nominally 50 km resolution SASS data and up to 5-8 km resolution from ERS-1 data were generated with the technique on a square grid of 14 pixels/deg latitude and longitude.

Resolution enhancement is not without cost; for instance, noise in the $\mathcal{A}$ images increases as resolution is increased. Hence, a tradeoff is made between the resolution and the noise level. Furthermore, multiple passes (which may take several days) over the target are required to obtain sufficient measurement overlap. The resolution enhancement is dependent upon the number of measurements with greater numbers contributing to a reduced estimate of noise and/or improved resolution. However, during the "imaging time interval" the target's radar characteristics must remain constant between passes. Some tradeoff must therefore be made between the imaging time interval and resolution when there is temporal change in the target, i.e., $\mathcal{A}$ and $\mathcal{B}$ should remain constant over the imaging time interval. For a sufficiently short interval this assumption is justified. However, ice motion and changing conditions limit the period for which it is true. For example, some diurnal variations in ice conditions can be expected. Unfortunately, because of the limited range of time-of-day observations in the scatterometer data, a full study of the diurnal variations of the backscatter is difficult and is not treated in this paper. Since this study was conducted during the winter period, any diurnal variations in the backscatter will be quite small. These and any other variations in σ^o during the imaging time interval are treated as noise by the image reconstruction algorithm. In the image time series used in this paper, 6 days of data were used to construct each image. The resulting images reflect an *average* surface response during this time period. Ice motion during the imaging time interval results in some image smearing which is most noticable along the ice edge.

In the general SIRF algorithm both $\mathcal{A}$ and $\mathcal{B}$ are estimated for each pixel. This requires σ^o measurements spanning a sufficiently wide range of incidence angles for each pixel. However, with the short imaging time interval used in this paper some pixels had inadequate σ^o incidence diversity to estimate $\mathcal{A}$ and $\mathcal{B}$ at the desired resolution. In applying the imaging technique, the resolution enhancement algorithm was modified to use a uniform $\mathcal{B}$ value for each pixel. Thus, only images of $\mathcal{A}$ were generated. The value of $\mathcal{B}$ used was determined by first collecting all the σ^o measurements over a large test area. The area was selected to include samples of each of the responses observed. Linear regression of the σ^o measurements versus incidence angle was then used to determine the nominal $\mathcal{B}$ value. While using a constant $\mathcal{B}$ in the imaging algorithm will introduce errors in the estimated $\mathcal{A}$ value, because of the small range (0.1 to 0.3 dB/°) of $\mathcal{B}$ the maximum error in $\mathcal{A}$ is generally less than 1 dB. A later paper will present SIRF images of both $\mathcal{A}$ and $\mathcal{B}$ values.

IV. SASS IMAGE TIME SERIES

SASS σ^o data span a range of $0° \leq \theta \leq 70°$; however, only measurements between 23° and 55° were used to create the images in this study. Measurements with excessive noise, (*i.e.* those with normalized standard deviations greater than 15%), were not used in the imaging process. Data from orbits with large spacecraft attitude errors were also rejected. The $\mathcal{B}$ value was assumed to be 0.2 dB/°.

While SASS made both vertically (vv) and horizontally (hh) polarized Ku-band (14.6 GHz) measurements of σ^o, only vertically-polarized σ^o measurements were used in this paper. Using the modified SIRF algorithm, a time series of $\mathcal{A}$ images of Antarctic sea ice was generated. The full 17 image time series covers JD 182 through JD 282 in 1978 (the time period of the Seasat mission) with each image corresponding to a 6 day period. Three images selected from this time series over the Weddell Sea are shown in Fig. 1. (Note that the resolution of the original images was degraded to make these reproductions. The black spots are areas not covered by scatterometer measurements during the six day imaging time interval.)

Examination of the images in Fig. 1 reveals significant spatial and temporal variation in $\mathcal{A}$. The criss-cross pattern at the top of each image corresponds to the open ocean. The location of the ice edge is readily discernible in these images as the southern limit of the criss-cross pattern. The Antarctic peninsula is visible as the bright tongue (with a dark "backbone") just left of center. Note that at Ku-band glacial ice is generally brighter (i.e., has a higher $\mathcal{A}$ value) than sea ice. The actual brightness (in winter) of the glacial ice is dependent on the snow thickness and interannual layering (see [3]). The large bright spots in the Weddell Sea appear to be tabular icebergs within the ice pack. In the Weddell Sea area we note large spatial and temporal variations in $\mathcal{A}$ which appear to correspond to circulation patterns.

We note that the ranges of values of σ^o over the ice

pack are less than the values observed by [5]. A casual examination reveals that there are two extreme ranges of $\mathcal{A}$ values evident in the sea ice images: the brightest areas have nominal $\mathcal{A}$ values of -14 to -10 dB while the darkest regions are -20 to -18 dB. This range may be compared with the -8 ± 2 dB for multi-year ice and -24 ± 4 dB for first-year ice suggested by Onstott [1992]. We note that the image pixel values correspond to the spatial (over the pixel area) and temporal (over a 6 day period) average. Thus, given the relatively coarse resolution of the scatterometer pixels (3-5 km) it is likely that the observed $\mathcal{A}$ values correspond to a mix of first-year and multi-year ice as well as open water. In this case, the observed value will tend to fall between the extremes suggested for the first-year and multi-year ice. Further, thermodynamic interactions of the ocean and ice will affect the radar brightness. It is likely that this is one of the primary mechanisms responsible for the observed circulation patterns in the radar response.

In a simple experiment to study ice motion using the SASS $\mathcal{A}$ images, each of several of these "tabular icebergs" were manually located in each image of the SASS time series. Two points on each target were located to enable study of their changing orientation. Several points along the edges of the dark regions were also tracked. A sample output is shown in Fig. 2. Target locations for each image are shown as solid lines with dotted lines interconnecting corresponding locations. The observed clockwise rotation is consistent with the Weddell Sea gyre. Further analysis of these images continues.

V. ERS-1 IMAGE TIME SERIES

The ERS-1 σ^o data span a range of $17° \leq \theta \leq 65°$. All available ERS-1 scatterometer measurements which did not have error flags were used to create images using the AVE algorithm. The $\mathcal{B}$ value used was 0.22 dB/°. Unfortunately, because of spatial filtering applied in the ground processing of the ERS-1 σ^o measurements, the possible resolution enhancement is significantly less than that of SASS. The resolution is also reduced due to more limited coverage resulting from ERS-1's single side operation. Nevertheless, we have successfully created enhanced resolution imagery from the C-band (5.2 GHz) ERS-1 data.

An image time series covering the same seasonal period of the SASS data (but 14 years later) was generated. Each image covers a 6 day period corresponding to the SASS images. Three images selected from this time series (over the Weddell Sea) are shown in Fig. 3. As in the SASS data, the images reveal significant spatial and temporal variation in $\mathcal{A}$ though the apparent resolution is significantly reduced. However, we note significant differences in the pattern of $\mathcal{A}$ brightness in the Weddell Sea from the SASS images. Most of these differences are attributed to interannual variability. However, the differing scattering characteristics between Ku-band and C-band may also be a factor. For example, the reduced resolution of the ERS-1 images may preclude location of tabular icebergs. Further analysis of these images continues.

VI. DISCUSSIONS AND CONCLUSIONS

While SASS data is over a decade old, it provides a unique historical data set to study climate change. By using the enhanced resolution scatterometer imaging technique [4], we have been able to generate Ku-band (and C-band using ERS-1) images of $\mathcal{A}$ for Antarctic sea ice. Although these images have only "medium-scale" resolution (4-8 km), they provide an ice sheet-wide view of the changing radar backscatter of the ice during several months of 1978 (SASS) and 1993 (ERS-1). Since the radar backscatter can be related to ice conditions [6], the scatterometer images enable wide-area studies of the ice sheet. Thus, the scatterometer data, coupled with resolution enhancement algorithms, can be an effectively tool in studies of sea ice. We note that some of the limitations of the imaging technique can be overcome by suitably modifying future scatterometers (see [4]). For example, with a modified scatterometer, multiple orbit passes are not required and the resolution can be improved to as low as 1-2 km. Coupled with very frequent revisits and multiple-incidence angle observations, such scatterometer data can be expected to significantly enhance studies of polar ice.

ACKNOWLEGEMENTS

SASS GDR data were obtained from the PoDAAC at the Jet Propulsion Laboratory.

REFERENCES

[1] Drinkwater, M.R., LIMEX '87 Ice Surface Characteristics: Implications for C-band SAR Backscatter Signatures, *IEEE Transactions on Geoscience and Remote Sensing*, Vol. 27, No. 5, 501-513, 1989.

[2] Livingstone, C.E., and M.R. Drinkwater, Springtime C-band Backscatter Signatures of Labrador Sea Marginal Ice: Measurements versus Modeling Predictions, *IEEE Transactions on Geoscience and Remote Sensing*, Vol. 29, No. 1, 29-41, 1991.

[3] Long, D.G., M R. Drinkwater, Greenland Ice Sheet Surface Properties Observed by the Seasat-A Scatterometer at Enhanced Resolution, in press *Journal of Glaciology*, 1993.

[4] Long, D.G., P.J. Hardin, and P.T. Whiting, Resolution Enhancement of Spaceborne Scatterometer Data, *IEEE Trans. Geosci. Remote Sensing*, Vol. 31, No. 3, May 1993.

[5] Onstott, R.G., SAR and Scatterometer Signatures of Sea Ice, In *Microwave Remote Sensing of Sea Ice*, (Ed.) F.D. Carsey, American Geophysical Union, Geophysical Monograph 28,, Chapter 5, 73-104, 1992.

[6] Winebrenner, D.P., J. Bredow, M.R. Drinkwater, A.K. Fung, S.P. Gogineni, A.J. Gow, T.C. Grenfell, H.C. Han, J.K. Lee, J.A. Kong, S. Mudaliar, S. Nghiem, R.G. Onstott, D. Perovich, L. Tsang, and R.D. West, Microwave Sea Ice Signature Modelling, In *Microwave Remote Sensing of Sea Ice*, (Ed.) F.D. Carsey, American Geophysical Union, Geophysical Monograph 28,, Chapter 8, 137-175, 1992.

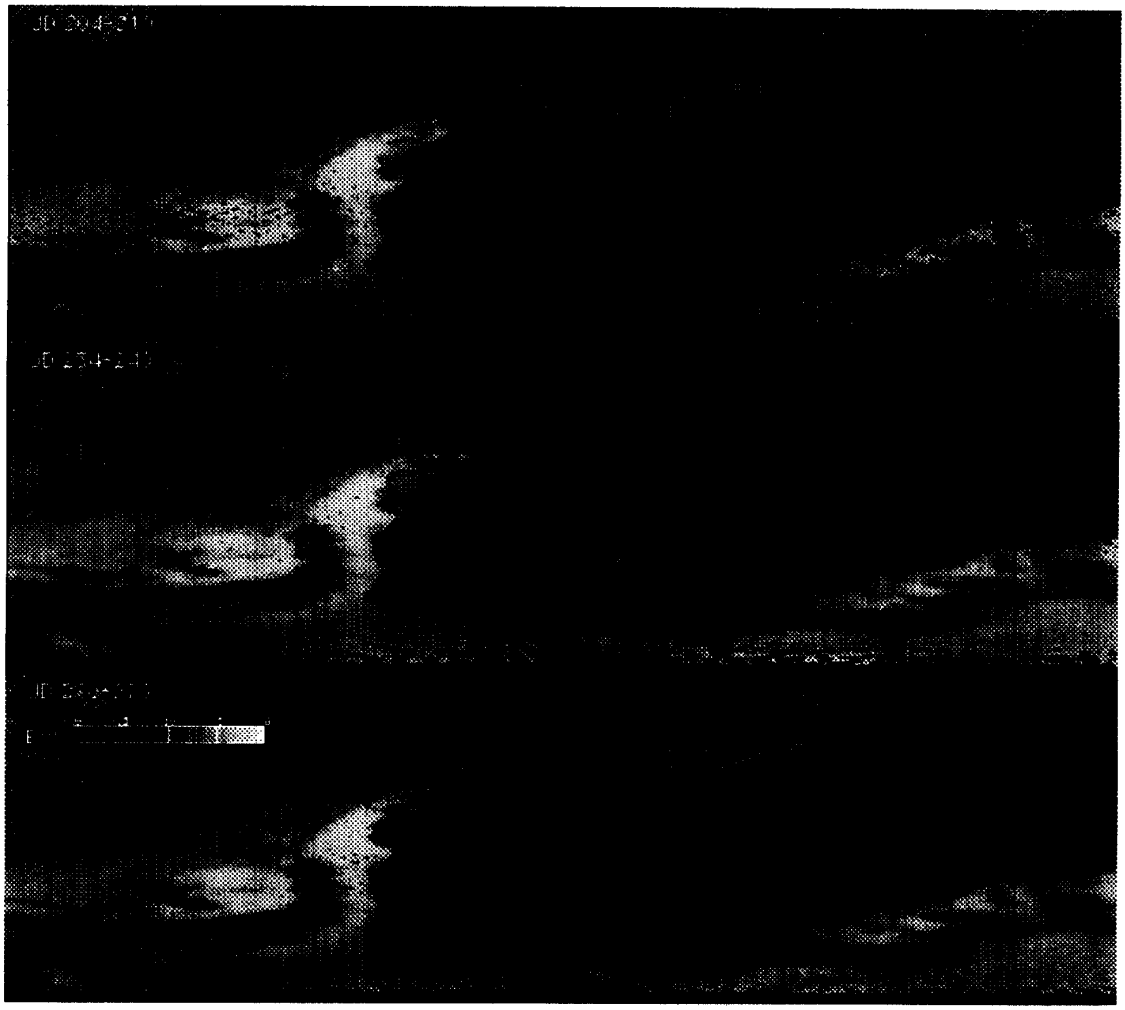

Figure 1. Selected images from a time series of $\mathcal{A}$ images (vv-pol) covering early July through early October 1978 from Ku-band SASS data. Each image covers a 6 day period. (a) JD 204-210. (b) JD 234-240. (c) JD 270-276. A rectangular lat/long projection was used.

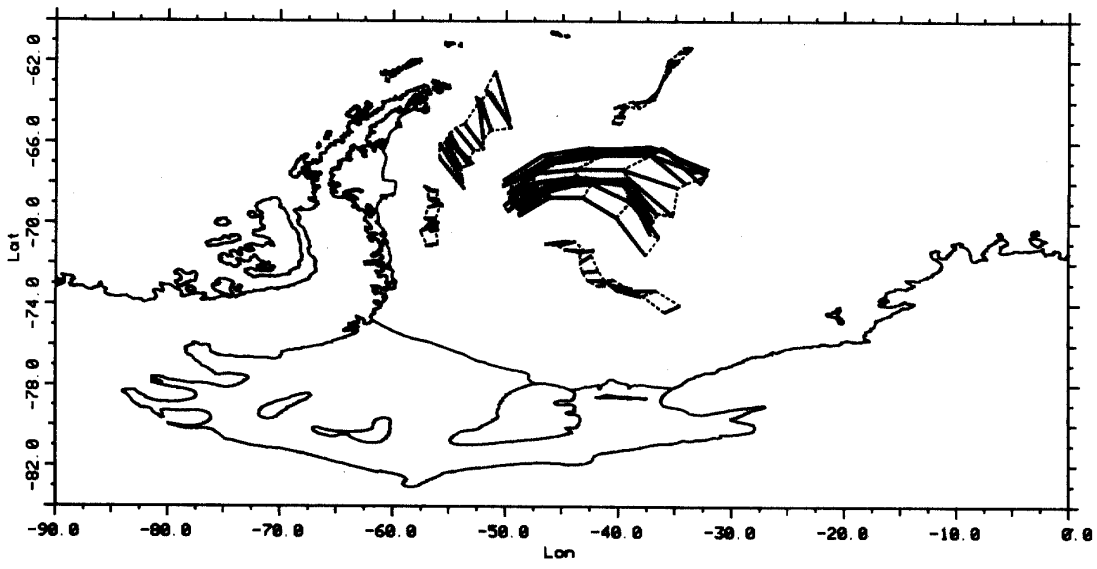

Figure 2. Map of the movement of selected features from the SASS image time series covering JD 181 through JD 282 in 1978.

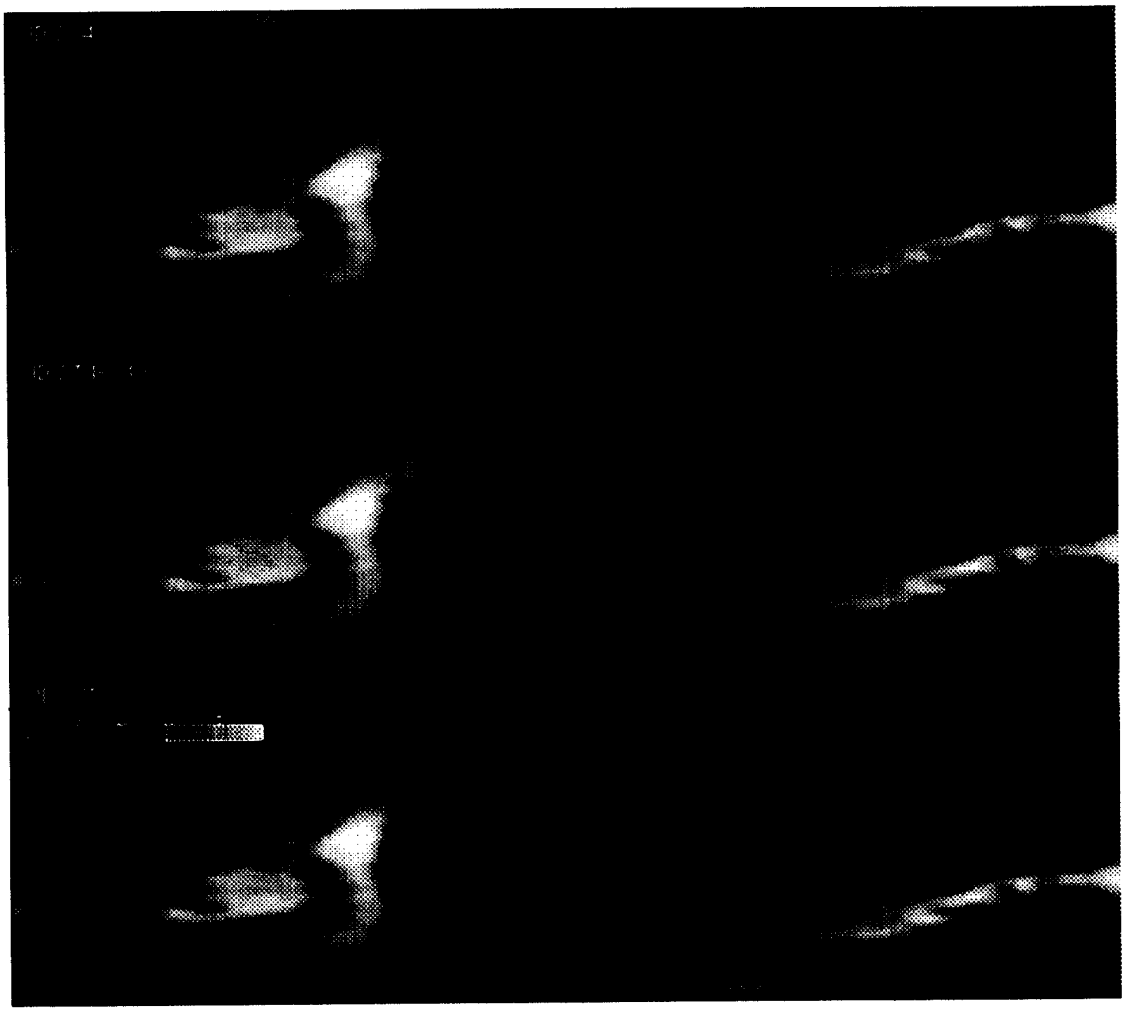

Figure 3. Selected images from a time series of $\mathcal{A}$ images (vv-pol) covering early July through early October 1993 from C-band ERS-1 data. Each image covers a 6 day period. (a) JD 204-210. (b) JD 234-240. (c) JD 270-276.